Machine Learning Predicts Pedestrian Wind Flow from Urban Morphology and Prevailing Wind Direction

Jiachen Lu[1,2,‡], Wei Li[2,‡], Sanaa Hobeichi[2,3], Shakir Aymam Azad[2], Negin Nazarian[1,2,3,*]

[1]School of Built Environment, UNSW Sydney, Sydney, NSW 2052, Australia.
[2]ARC Centre of Excellence for Climate Extremes, UNSW Sydney, Sydney, NSW 2052, Australia.
[3]ARC Centre of Excellence for 21st Century Weather, UNSW Sydney, Sydney, NSW 2052, Australia.
[‡]These authors contributed equally to this work.
[*]Corresponding author: n.nazarian@unsw.edu.au

Abstract.

Pedestrian-level wind plays a critical role in shaping the urban microclimate and is significantly influenced by urban form and geometry. The most common method for determining spatial wind speed patterns in cities relies on numerical computational fluid dynamics (CFD) simulations, which resolve Navier-Stokes equations around buildings. While effective, these simulations are computationally intensive and require specialised expertise, limiting their broader applicability. To address these limitations, this study proposes a more cost-effective alternative while maintaining the accuracy and spatial patterns captured by CFD. We developed a machine learning (ML) approach to predict wind speed patterns from prevailing wind directions and three-dimensional urban morphology, which are increasingly available for global cities. The model is trained and tested using a comprehensive dataset of 512 numerical simulations of urban neighbourhoods, representing diverse morphological configurations in cities worldwide. We find that the ML algorithm accurately predicts complex wind patterns, achieving a normalised mean absolute error of less than 10%, which is comparable to wind anemometer measurement in a low wind speed environment. In predicting wind statistics, the ML model also surpasses that of regression models based solely on statistical representations of urban morphology. The R^2 values measuring grid-level agreement between ML and CFD range from 0.94-0.99 and 0.65-0.95, respectively, for the idealised and whole datasets. However, we find that grid-based R^2 is not an effective metric for evaluating the 2D model performance due to localised biases arising from faster wind speed grid regions, which is revealed by the wind probability density function. This further confirms the suitability of the ML models for capturing wind distributions at pedestrian height. These findings demonstrate that complex pedestrian wind patterns can be effectively predicted using an image-based ML approach, circumventing the need to resolve complex physical equations directly.

Keywords: urban wind speed estimation, urban climate modelling, machine learning

1. Introduction

The urban environment is a complex system with three-dimensional changes in form, fabric, and function. The complexity results in high spatial variabilities in microclimate, modified by heterogeneous urban morphology as well as anthropogenic fluxes of heat and pollutants (Krayenhoff et al., 2021). The urban microclimate also exhibits diurnal and seasonal variations, making urban meteorology a dynamic field that requires continuous monitoring and evaluation.

Physical and numerical modelling is the most common approach in studying urban climate across scales. Based on applications and the scale of interest, urban processes can either be explicitly resolved by computational fluid dynamics (CFD) models (Takemi et al., 2020) for microclimate or be parameterised in urban land surface models (ULSMs) for general interaction between the urban area and the upper atmosphere (Lipson et al., 2018). In between, the coupling framework connecting CFD models and ULSMs provides better boundary conditions and forcings for downscaling tasks (Lin et al., 2021) as well as upscaling of microscale urban data for large-scale models (Creutzig et al., 2019). While the coupling has promoted a more accurate and efficient evaluation of urban microclimate, most studies were focused on specific areas and meteorological conditions (e.g., (Bechtel et al., 2012)) of a period, which limits generalisations and reuse of the flow field for cities of a great variance (Boeing, 2019). Such a limitation has incurred repetitive efforts to rerun computationally expensive simulations for evolving urban environments (e.g., (Santiago et al., 2017)).

Recent advancements in accessibility to realistic urban geometry (Sirko et al., 2021), as well as computational power, have facilitated an unprecedented number of urban airflow datasets (e.g., (Kanda et al., 2013)). Efforts in gathering, harmonising, and employing urban information have also emerged as an efficient approach to addressing urban challenges (urban climate informatics (UCI) (Middel et al., 2022)). For example, urban canopy parametrisations (UCPs) is developed by correlating urban geometrical conditions to the corresponding fluxes to the atmosphere (Nazarian et al., 2020), enhancing the representation of building effects (Martilli et al., 2002) in mesoscale climate models. However, UCPs have inherent limitations from their city representations and flow homogeneity assumption, which blocks further probing into building-scale ($\leq$ 100m) urban environments (Chen et al., 2022a) that is relevant to thermal comfort studies (Nazarian et al., 2019).

The success of machine learning (ML) and neural networks (NNs) in image processing, particularly computer vision techniques, has motivated numerous urban applications using ML for object detection, classification, and regression tasks. Convolutional NNs (CNNs) are the predominant models employed for this purpose with convolutional layers encoding key spatial features from input images and supplying the feature to subsequent layers to perform the required tasks. For instance, based on satellite images over cities, CNN has helped to identify and locate building footprints (Sirko et al., 2021), and to estimate building heights (Cao et al., 2021) that collectively

reconstruct 3D urban geometry. The satellite image can also be generalised for climate modelling purposes, where CNN helped to classify local climate zone (LCZ) (Liu et al., 2020). Starting from urban flow datasets, NN can be developed as a surrogate model trained on urban factors and resulting urban microclimate to emulate urban processes. The high efficiency of these models has boosted downscaling approaches to city scale of sub-hectometres for urban environment (Briegel et al., 2023; Bechtel et al., 2012).

Unlike temperature and heat fluxes generally following seasonal and diurnal cycle (Ha et al., 2020), the urban wind speed is more variable (Droste et al., 2018) and subject to interactions between the urban boundary layer and urban configurations (Oke et al., 2017). Under neutral conditions, urban wind speed field can be expressed as $U = f(\phi_h, \phi_v, \phi_\alpha)$, where ϕ_h represents urban horizontal geometry such as building footprint and street orientations (Lu et al., 2023a), ϕ_v represents building height variability that consists major urban vertical heterogeneity (Lu et al., 2024b), and ϕ_α reflects mesoscale forcings such as the strength and direction of the prevailing wind (Santiago et al., 2013). The complexities of the urban wind field have constrained its physical modelling to a neighbourhood scale of limited scenarios (e.g., (Letzel et al., 2012)). However, wind fields are a major factor in many urban applications. For example, a) the increase in wind speed contributes to better pedestrian thermal comfort in heatwave events (Lam et al., 2018) but attracts a great discomfort in cold climate regions (Liu et al., 2022); b) the wind speed pattern within urban canopy reflects its ventilation efficiency (Ng et al., 2011) that is likely worsens amid urbanisation, which requires active evaluation for urban planning decisions altering the air paths; and c) wind speed is an essential meteorological input to drive the land surface models (Best et al., 2015) in characterising flow transport, which constitutes a major contribution of urban feedback to climate models.

Several ML approaches based on different datasets and applications have shown to be successful while also manifesting limitations in several aspects: firstly, some models were trained on idealised urban arrays with random distribution (e.g., (Lu et al., 2023b)), which is particularly limiting due to the 3D complexity of realistic urban morphology. Secondly, the performance of the NN model directly connects to the host dataset for training and testing. However, most training (e.g., (Chockalingam et al., 2023)) relies on a limited dataset without considering neighbourhoods of global cities, which constrains general use beyond their area of interest. Finally, some models, such as that by Mokhtar et al., 2021, were developed outside the specific context of urban climatology, meaning their performance metrics may not be fully suitable to address real-world urban climate applications. While being outside the urban climate domain does not inherently diminish their value, the lack of metrics specifically designed for urban settings such as wind extremes questions their applicability and accuracy in addressing urban climate issues.

This study aims to address these limitations using the recent development of a comprehensive, high-resolution urban flow dataset (UrbanTALES (Nazarian et al., 2024)), developing and evaluating a neural network model to predict pedestrian-level

wind fields. The model is designed to map both realistic urban geometry over flat terrain and prevailing wind directions to the resulting wind field. Further, we focus on predicting the spatial patterns of pedestrian wind speed, addressing the following research questions:

- Can the ML approaches replace CFD simulations for predicting mean wind speed at the pedestrian level?
- How is the performance of the ML model impacted by the underlying dataset?

The paper is organised as follows, Sect. 2 describes the numerical setup of large-eddy simulation (LES) used to prepare the training and testing dataset and the NN model to emulate the physical process and predict pedestrian wind speed field. Sect. 2.3 depicts the transformation and processing of airflow data between LES and NNs. Sect. 3 demonstrates the model performance in metrics on urban applications. Sect. 4 raises conclusions remarks and perspectives.

2. Methods

We use an extensive LES dataset (described in Sect. 2.1) to train and test a prediction model for the distribution of pedestrian wind speed responding to the urban geometry and prevailing wind directions. The ML approach used here is CNNs, described in Sect. 2.2, and followed by the (pre and post) data processing methods in Sect. 2.3. Figure 1 demonstrates the dataset and data processing procedure, which will be explained in this section.

2.1. Dataset Formulation and Large-eddy Simulation

The ML model was trained based on UrbanTALES (Nazarian et al., 2024) - an extensive high-resolution urban flow dataset covering both idealised building blocks and realistic neighbourhoods (Fig. 1(a)). We considered 224 idealised and 288 realistic cases in the dataset, which are constructed to cover a comprehensive range of urban morphologies seen in global cities. The idealised building blocks are built to cover eight urban densities ranging from $\lambda_p \in [0.06, 0.64]$, two commonly used horizontal configurations (aligned and staggered (Coceal et al., 2007)), and three building height distributions ($H_{\text{std}} \in [0, 2.8, 5.6]$m with the same mean building height $H_{\text{mean}} = 16$m). The realistic urban geometry is extracted from OpenStreetMap (OpenStreetMap contributors, 2017) using OSM2LES (Lu et al., 2022), with the level of details (LOD) 1.3 for urban geometries (Biljecki et al., 2016), where the small building parts were identified and extruded to the designated height level.

The numerical setup for the flow simulation is described in detail in Nazarian et al., 2024 and is noted here for completeness. The LES mode of the Parallelised Large-eddy Simulation Model (PALM, version r4554 (Maronga et al., 2020)) is used to perform simulations over urban geometries under neutral conditions. The only driver is

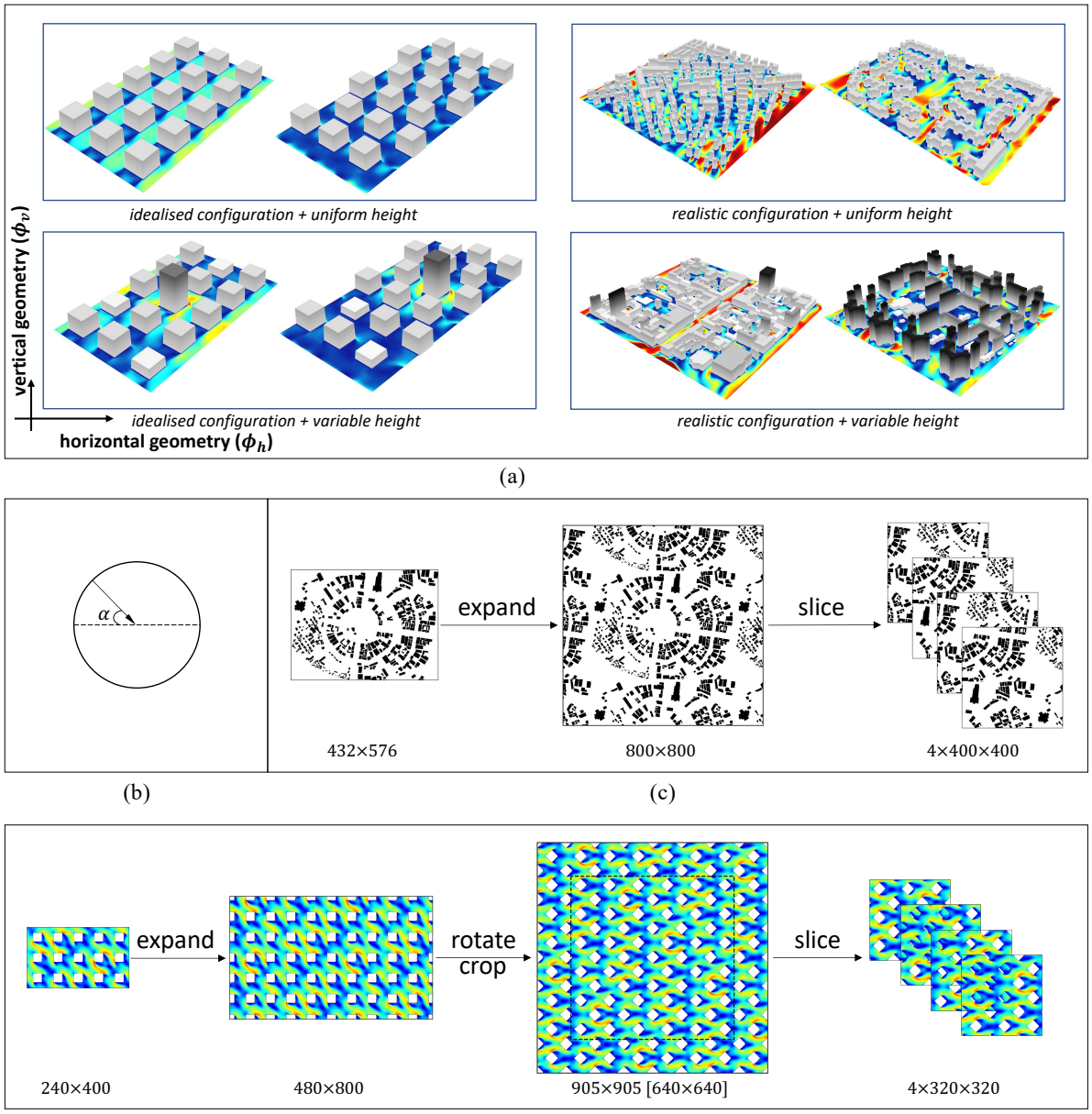

Figure 1: Dataset and data processing workflow. (a) Four types of urban configurations are considered in UrbanTALES representing horizontal (ϕ_h) and vertical (ϕ_v) variation in the building geometry. b) In addition to geometry variations, prevailing wind directions α are varied in the flow dataset while the strength of the pressure gradient ($\frac{dp}{dy} = \frac{dp}{dx}\tan\alpha$) driving the flow is the same. (c) Data preprocessing to make the flow field from numerical simulations compatible with ML workflow for orthogonal α. The flow field of varying sizes in cases was first expanded based on the lateral periodic boundary conditions to a uniform size of 800×800m and sliced to four 400×400m. (d) The prepossessing procedure shown for an idealised configuration with oblique wind direction ($\alpha = 45^o$). Colours represent the pedestrian wind speed.

a constant pressure gradient of magnitude $\sqrt{\left(\frac{\partial p}{\partial x}\right)^2 + \left(\frac{\partial p}{\partial y}\right)^2} = A_a(z)\rho u_\tau^2 / V_{\text{air}} \approx \rho u_\tau^2 / H_T$ where $A_a(z)$ is the surface area of air at z height level, ρ is the air density, u_τ is the friction velocity, and V_{air} is the total volume of air in the numerical domain. We keep the friction velocity $u_\tau \approx 0.21$m/s the same for variable prevailing wind direction and vary the partitioning between pressure gradient at x and y direction. The Reynolds number $Re_\tau = u_\tau H_T / \nu \approx 2.5 \times 10^6$ is large enough to neglect viscosity effects and independent of Reynolds number effects.

The time-averaged wind speed field ($U = \sqrt{\overline{u}^2 + \overline{v}^2 + \overline{w}^2}$, where $\bar{\cdot}$ indicates time-averaged flow properties, u, v, and w are streamwise, spanwise, and vertical velocity, respectively sampled at the pedestrian ($z = 1.5$m) level (examples are shown in Fig. 1(a)).

Note that the present study built a mapping between urban configurations and the corresponding wind field with imagery features that reflect the flow pattern around buildings. Other urban climate parameters, including mean radiant temperature and thermal comfort indices, which reflect thermal comfort levels, as well as turbulent momentum and heat flux, which assess urban responses to atmospheric flow, can also be predicted using the same framework. This approach allows for comprehensive modelling of urban climate dynamics and their interactions with the atmosphere.

2.2. Convolutional Neural Network Models

While UrbanTALES is a comprehensive LES dataset with expansive coverage of urban configurations and densities, the number of cases is still limited for ML algorithms. Considering this we adopt the U-net model introduced by Ronneberger et al., 2015 as a type of CNNs that was originally designed for biomedical image segmentation and optimised for small datasets, which has been proved effective in urban wind speed predictions (Lu et al., 2023b). In our case, the generic U-net model is adjusted to further match the purpose where the details are shown in Appendix A. The model is implemented using the PyTorch backend (Paszke et al., 2019) and trained on two NVIDIA Tesla V100 graphics processing units (GPUs) with mean absolute error (MAE) loss function and the Adam optimiser (Kingma et al., 2017). Similar to Lu et al., 2023b, we train the model for 1,000 iterations with a fixed learning rate of 0.001 and a batch size of 16.

2.3. Data Processing

As a CNN model, U-net requires uniformity in the input image sizes. The raw LES domain sizes, however, vary in size as they represent realistic urban geometries with varying boundaries. The following explains the pre-processing and post-processing of the images (2D array of values representing urban geometries and pedestrian wind speeds) in the dataset to achieve uniform image sizes for the model.

Data Pre-processing for machine learning It is crucial to ensure the physical meaning of values remain meaningful in the data processing stage. The common practice is to expand the images by padding constant values, such as zeros, to the original images. However, the periodic boundary conditions imposed during LES simulations in our case can help better expand the images, where the wind field can be padded with the wrap of the 2D image along both axes. This procedure helps make sure that the image is augmented while the underlying physics is also preserved. Details are shown in Fig. 1(b-c) and explained in detail in Appendix B.

Data Post-processing Two post-training tasks are necessary to restore the output from ML workflow to the original LES flow field. The first one is essentially a reverse procedure of the pre-processing steps and the second is to clean up unphysical predicted values such as non-zero wind speeds within the buildings. An example of this procedure is shown in Appendix B.

2.4. Experimental setup and performance metrics

The split of train and test data needs to be random to ensure objectivity. In each experiment, we allocate ∼80% of the data for training and ∼20% for testing. While, the prediction model does give a full 2D wind field, different urban applications care about different aspects of the wind field. For example, thermal comfort and ventilation (e.g., (Nazarian et al., 2019)) studies may require detailed wind speed patterns, while disaster prevention (Duan et al., 2021) and land surface modelling applications (Harman et al., 2004) rely on the extreme and aggregated value, respectively. Therefore, model skill varies when used for different applications and we will evaluate the performance in three independent metrics as follows,

$$\text{(i)}\ \ \mathrm{R}^2 = 1 - \frac{\sum_{i=1}^{N}(U_i - \hat{U}_i)^2}{\sum_{i=1}^{N}(U_i - \bar{U})^2},$$

$$\text{(ii)}\ \mathrm{NMAE} = \frac{\sum_{i=1}^{N}|U_i - \hat{U}_i|}{N\sum_{i=1}^{N}U_i},$$

$$\text{(iii)}\epsilon_\sigma = \frac{|\sigma - \hat{\sigma}|}{\sigma},$$

Where N is the total number of image pixels corresponding to the wind speed (i.e. excluding building pixels), U_i is the true wind speed from LES at pixel i, $\hat{U}_i$ is the corresponding predicted wind speed, and $\bar{U}$ is the mean of the true wind speed. For the relative standard deviation error, ϵ_σ, σ is the standard deviation of the true wind speed, and $\hat{\cdot}$ denotes the predicted values.

(i) **Determination coefficient ($\mathbf{R}^2$)**: to measure how well the predictions explain variability in the truth. However, some minor defects such as the flow pattern being shifted down/upstream will significantly reduce R^2.

(ii) **Normalised mean absolute error (NMAE)**: to test if the ML model captures the flow pattern distribution but fails in giving a correct magnitude. Cases showing unanimous over or underestimation of wind speed can be then amended by globally subtracting or adding a value.

(iii) **Relative standard deviation error (ϵ_σ)**: the standard deviation, when combined with MAE, depicts the general statistical distribution or probability density function (PDF) of the wind speed map. ϵ_σ then can help measure the spread of wind speed values and the typical distance between wind speed at each data point and the mean.

3. Results and Discussion

Although urban geometry data is becoming increasingly available (Li et al., 2024), obtaining this information on a global scale remains challenging (Herfort et al., 2023). Therefore, we conduct two sets of experiments corresponding to two common scenarios based on how much urban geometry information is available: The first approach focuses on idealised urban configurations (Sect. 3.1). When the detailed 3D urban geometry is not available, some parameters such as plan area density (λ_p) and building height distribution statistics (such as mean building height and standard deviation of building height) are given. In this case, the best practice is to construct a set of idealised urban arrays matching these parameters as a surrogate (e.g., (Wang et al., 2021)). Second, we detail the performance of the prediction model when detailed urban geometry datasets are available, combining the entire dataset of idealised and realistic configurations (Sect. 3.2).

3.1. Prediction over Idealised Urban Arrays

Here we consider idealised urban arrays in the UrbanTALES dataset with one uniform and three building height distributions (Lu et al., 2024b), namely *continuous*, *clustered*, and *high-rise* configurations. The robustness of various training and test data splits is demonstrated by conducting 20 experiments using different random seeds to divide the data (results are shown in the supplementary file). The R^2 scores for the training and test sets hover around 0.94 and 0.99, respectively, which indicates the model performance is irrespective of the seed (test results are shown in Appendix C).

Figure 2 illustrates the distribution of performance metrics for the train and test sets and categorised by prevailing wind angle. The prediction model is capable of capturing the wind speed with high accuracy as evidenced by the low and concentrated NMAE (mostly below 10 %, which is lower than typical wind speed measurements from modern anemometers (Azorin-Molina et al., 2023) at low wind speeds where the signal-to-noise ratio is low) and high R^2 (mostly above 0.9). Additionally, the model performance is close between the training and test data, indicating that it generalises well to the out-of-sample scenarios. The statistical metrics (ϵ_σ) are wider spread, which indicates

variations in the training data have a higher impact on the statistics of the wind field. The impact of prevailing wind direction on the model performance is overall minor where the $\alpha = 45^o$ shows greater variance in all three metrics.

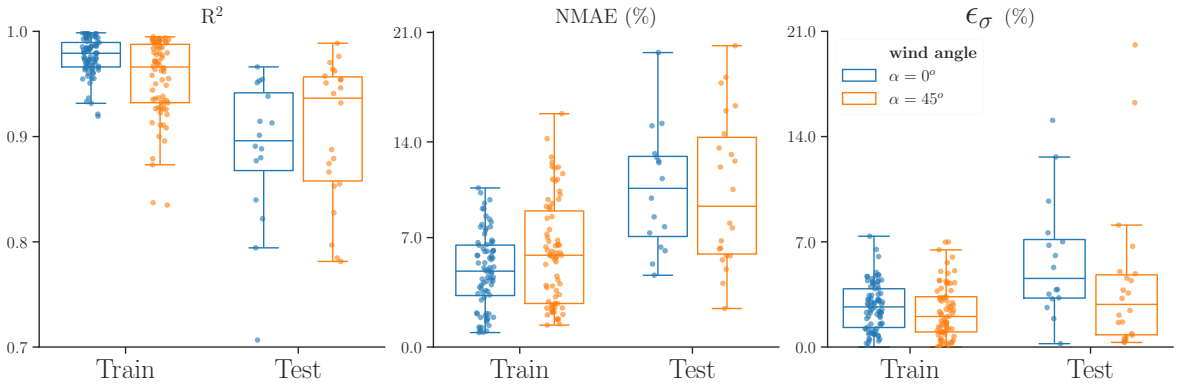

Figure 2: Performance of the ML algorithm trained with the idealised urban layouts. Three model performance metrics (Sect. 2.4) are shown for the training and test sets. The box plots are categorised by prevailing wind angle $\alpha = 0^o$ (blue) and $\alpha = 45^o$ (orange).

To showcase the model skill over the wind field pattern, we select three pairs ($\alpha \in [0^o, 45^o]$) of cases corresponding to three building height distributions from the test set in Fig. 3. The selection is also considered to cover three urban densities ($\lambda_p \in [0.0625, 0.25, 0.4444]$) and reflect intermediate model performance.

The first pair in Fig. 3 shows the comparison for the *clustered-aligned* urban layout. The differences in building heights result in unevenly distributed wind fields around individual building blocks where the flow around tall buildings has faster wind speed due to the enhanced vertical transport of momentum (Xie et al., 2008). The prediction model was able to reproduce the typical double-peak wind speed distribution commonly seen in aligned urban layouts, where the first peak ($U \approx 0.2$m/s) representing the leeward facets cavity (size and wind speed) is accurately captured. This capacity in particular benefits identifying the strong building leeward vortex that significantly worsens the ventilation of particles out of the urban canyons (Mei et al., 2018). However, the prediction systematically underestimated the wind speed in the wind corridor ($U \approx 0.8$m/s) and the wake region ($U \approx 1.2$m/s), which contributed to an underpredicted wind speed PDF at the second peak. For the oblique wind direction ($\alpha = 45^o$) case, the double peak behaviour remains, the cavity region is larger but encloses higher wind speed. The prediction shows a similar behaviour of the $\alpha = 0^o$ layout but overestimates the windward recirculation region. It also underestimates the wind magnitude within the wake, leading to a poor capture of the wind maxima.

The second pair shows *high-rise staggered* urban layout result with medium density ($\lambda_p = 0.25$). The PDF of wind speed shows a skewed Gaussian distribution towards the lower end ($U \approx 0.1$m/s). The prediction model captures the overall flow pattern well

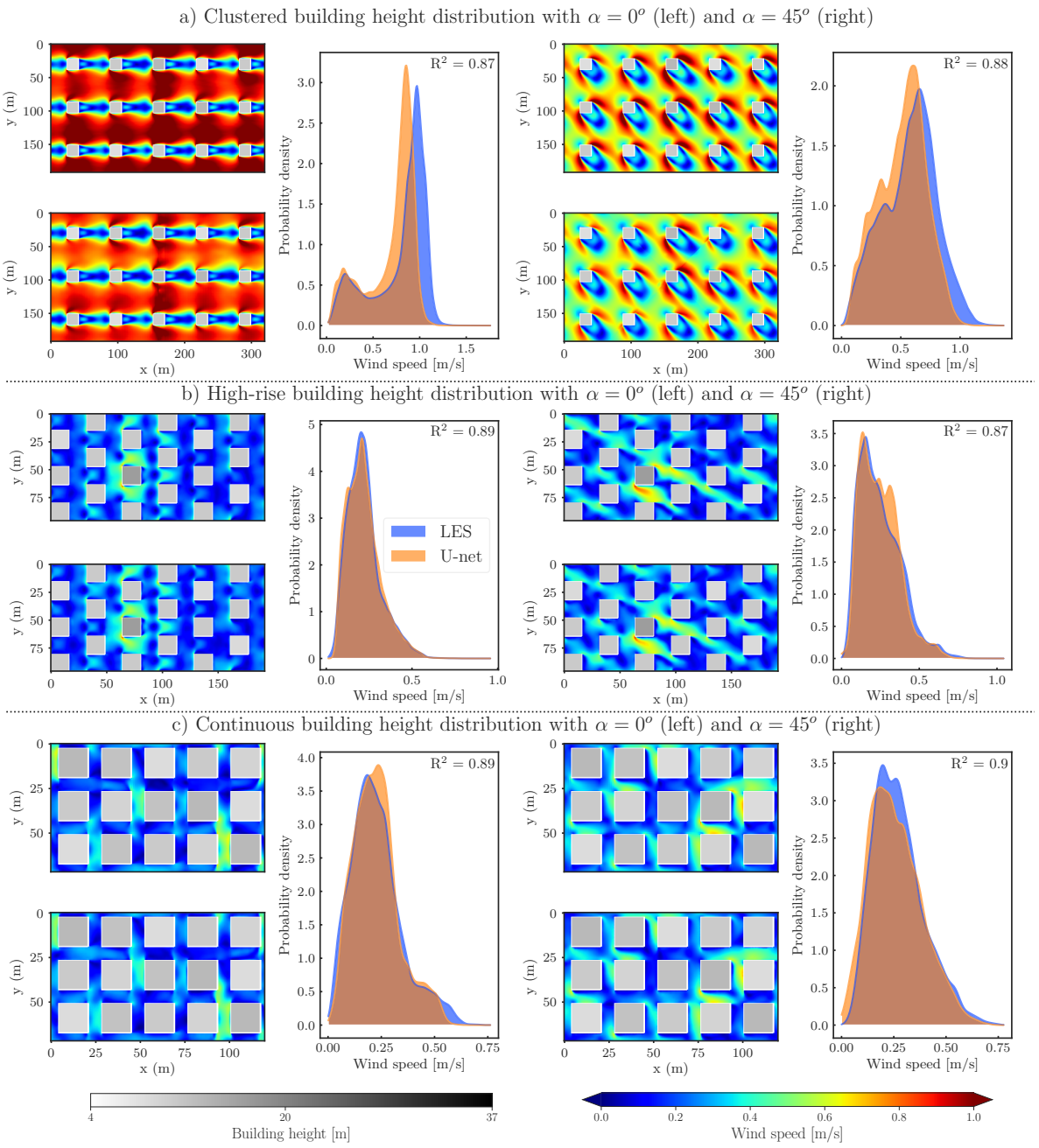

Figure 3: Comparison of wind speed field from (LES, upper plot in each comparison) model with (ML, lower plot in each comparison) predictions (only trained with idealised urban layouts in UrbanTALES) for three pairs of cases from the test set for sparse ($\lambda_p = 0.0625$), medium ($\lambda_p = 0.25$), and dense ($\lambda_p = 0.4444$) layouts. In total, six cases are presented, with configurations and angles indicated by the vertical titles. Height and wind speed colour bars are shared between the LES results and predictions.

for the $\alpha = 0^o$ scenario but produces an artificial second peak at $U \approx 0.3$m/s for the $\alpha = 45^o$ scenario. Meanwhile, the prediction misses some extreme values at both the

high ($U \approx 0.7$m/s) and low ($U \approx 0$m/s) ends and therefore may face challenges when the objective is to capture extreme values for thermal comfort and urban ventilation assessment (Ng et al., 2011). One possible way to improve the prediction capacity of the distribution tail is by modifying the loss function to penalise the model for incorrectly predicting the low and high extremes (Bittner et al., 2023).

The third pair demonstrates the model performance over a dense *continuous aligned* configuration. The fastest wind speed ($U \approx 0.58$m/s) occurs at the windward facet of the two tallest buildings for the $\alpha = 0^o$ case. The predicted wind field captures the position of this wind extreme but overlooks the magnitude. On the other end of the distribution, the model accurately placed the low wind speed region but overestimated its value. As a result, the PDF is squeezed towards the mean. For the oblique wind ($\alpha = 45^o$) configuration, similar to the other two pairs, the R^2 score remains close to $\alpha = 0^o$, which could be attributed to changing wind direction not complicating the wind field.

The prediction model works well over two sets of idealised building arrays constructed following common urban morphological parameters. However, the realistic urban landscape featuring a great heterogeneity (Lu et al., 2023a) requires the actual urban morphology for evaluation, which will be addressed in the next section.

3.2. Prediction over both idealised and realistic urban neighbourhoods

For the scenario where the modeller is given detailed and realistic urban morphology, we train and test the model using the full version of UrbanTALES with 512 urban configurations, which include both idealised and realistic urban configurations. The R^2 scores for the training and test sets cluster around 0.95 and 0.65, respectively, which is similar to physical estimation approaches such as Wang et al., 2020. The distribution of performance metrics, separated by configurations, for the training and test sets, are shown in Fig. 4.

The performance of the model based on the whole dataset has slightly degraded, which is expected as the size of the training data might not be sufficient for the prediction model to learn the more realistic and complex flow patterns. In the test set, all three metrics are wider spread than the training, and the difference is larger for realistic configurations. While increased configuration diversity by using the full dataset poses challenges for generalisation, the model still yields satisfactory performance better than statistical methods (Wang et al., 2024) consuming similar computational power. This can be attributed to the ML model does not rely on fitting certain wind speed distribution functions (e.g., Weibull distribution in Wang et al., 2022), which provides better flexibility to accommodate realistic and complex wind fields.

The model performance over different urban configurations such as building densities and height variability (Fig. 1(a)) further reflects its generalisation skills. Figure 5 presents performance metrics over six density ranges. The train set maintains a high score across densities, which demonstrates the model's effective feature extraction

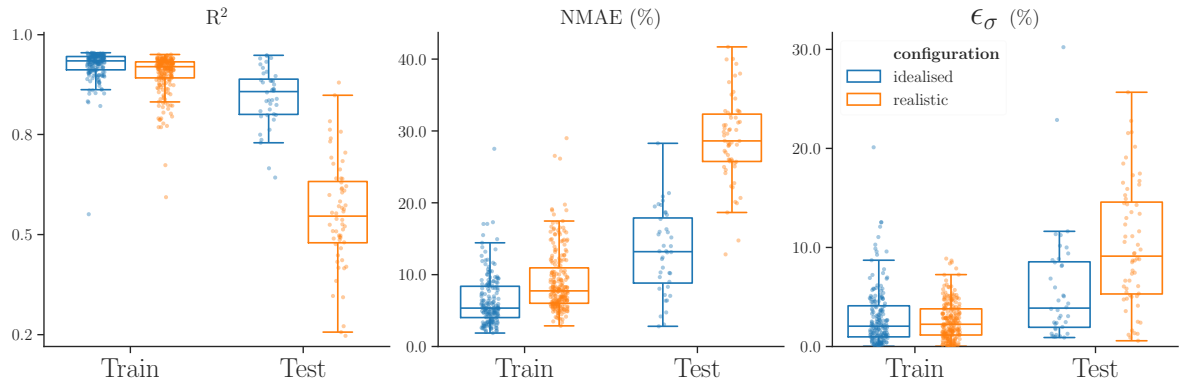

Figure 4: Performance of the ML algorithm trained with the entire UrbanTALES dataset consisting of idealised and realistic configurations (512 simulation cases). Three model performance metrics (Sect. 2.4) are shown for the training and test sets. The box plots are categorised by idealised building blocks (blue) and realistic urban neighbourhoods (orange).

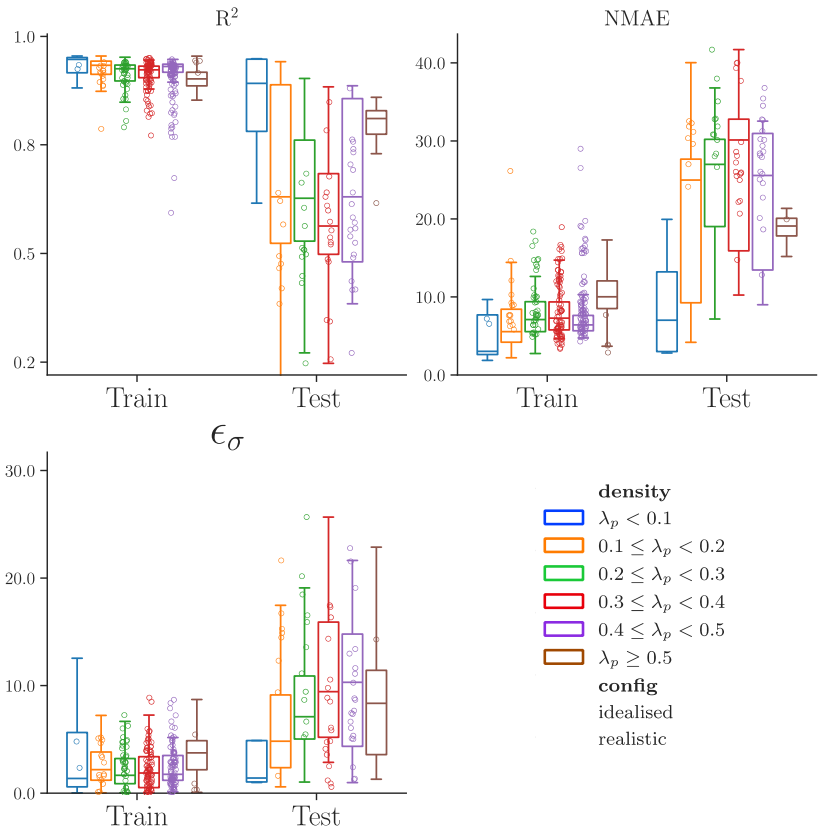

Figure 5: Performance evaluation for the prediction model based on the whole UrbanTALES dataset showing detailed distribution of model performance based on ranges of urban densities where the idealised (circle) and realistic (triangle) cases are distinguished by markers.

and pattern recognition capabilities in urban geometry, indicating robust spatial learning for wind speed prediction. The very sparse ($\lambda_p \leq 0.1$) and dense ($\lambda_p \geq 0.5$) categories mostly reflect model skills over idealised configurations since the density (λ_p) for realistic cases are centred around $[0.15 - 0.45]$. Within this range, the performance metrics show a general decreasing trend, which is expected since denser layouts lead to more complex flow (Lu et al., 2023a) that needs better generalisation.

The statistics of wind speed is sometimes a surrogate when the detailed flow field is not available (e.g., (Yuan et al., 2012)), and can be predicted from urban geometrical conditions (such as urban density and building height distribution, e.g., (Wang et al., 2020)). Next, we compare the performance of the ML model based on the 2D flow field and a non-linear regression model (baseline model thereafter) solely based on urban geometrical parameters and the resulting wind speed statistics. Figure 6 shows the mean (U_{mean}), standard deviation (U_{std}), and maximum (U_{max}) of the wind speed.

The baseline model considered here is trained based on the random forest model, i.e., an ensemble learning method that builds multiple decision trees during training and outputs the mean prediction of the individual trees to improve prediction accuracy and control over-fitting. The model maps inputs including *prevailing wind direction*, *plan area density*, *standard deviation of building heights*, and the *urban geometry configuration* to the output of wind speed statistics for individual cases. The split of training and test sets of the baseline model were kept identical to that of the prediction model to ensure consistency across predictions.

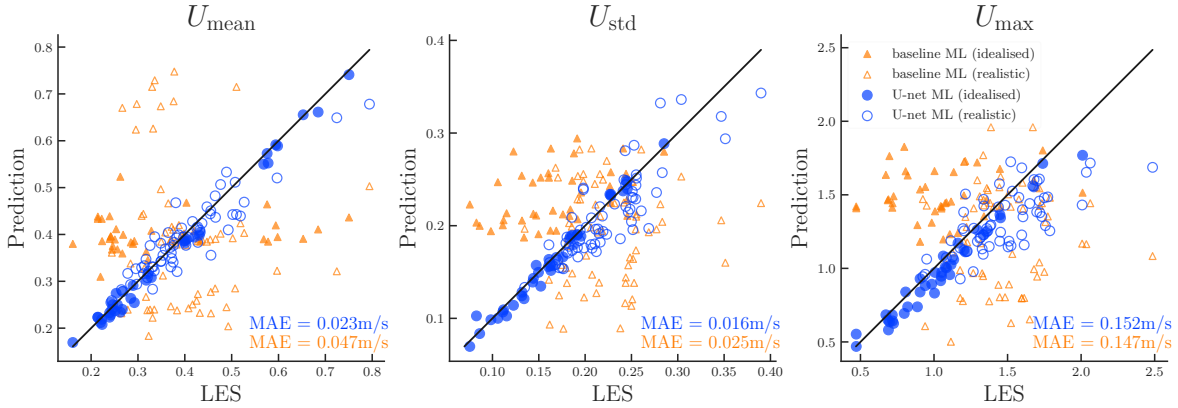

Figure 6: Scatter plot showing the model skills in predicting wind field statistics where the blue makers represent the U-net model trained on 2D urban geometry and orange represents the baseline model trained only on urban geometrical indicators.

The models are differentiated using distinct colours while urban configurations are shown with different markers in Fig. 6. The U-net predictions for U_{mean} and U_{std} are tightly clustered around identity line (Prediction equals LES), with very small MAE values (0.023m/s for U_{mean} and 0.016m/s for U_{std}), indicating close alignment with LES. In contrast, the baseline model prediction for U_{mean} and U_{std} are scattered and show a clear separation between realistic and idealised configurations. As opposed to

U_{mean} and U_{std} measuring the entire flow field statistics, U_{max} represent wind extremes, which usually sit near the building windward facets or in the lateral wakes (Lu et al., 2024b) and therefore is harder to capture. The U-net model performs better than the baseline model but with higher MAE because the model systematically underestimates the maximum values, particularly for the higher wind speed values. The baseline model is quite spread across the whole range and cancels errors calculated from mean bias. These behaviours can be explained as follows:

- The baseline model overestimate U_{mean} but underestimate U_{std} for realistic configurations. This is expected since the simple regression model is highly navigated by the variation in urban density, which shows a negative/positive correlation with $U_{\text{mean}}/U_{\text{std}}$ for idealised configuration (e.g., (Xie et al., 2008)). However, realistic urban geometries are highly variable in both horizontal and vertical geometrical aspects and the resulting flow field shows a weaker correlation to the conventional geometrical parameters (Lu et al., 2023a).
- The lower skill of the U-net model on U_{max} is also observed in Fig. 3 where the higher ends of wind speed distribution are missing from the prediction. The baseline model overestimates/underestimates U_{max} for idealised/realistic configuration, again, due to the unrealistic high weight of urban density, which shows a negative correlation (Nazarian et al., 2024) with U_{max} for idealised configurations.
- Given that the random forest model is not designed to capture the spatial features and dependencies of the input data, its performance declined with more complex configurations. In comparison, spatial characteristics were encoded as features in the U-net model, which enabled it to incorporate spatial information into learning and gain a better understanding of the physical flow patterns around buildings.

Similar to Sect. 3.1, we select six cases from the test set, and compare the LES results with the U-net predictions. The first row of Fig. 7 shows a comparison of two identical geometry over different prevailing wind directions. The second row further demonstrates how building height variability affects the model performance. The third row shows two examples of R^2 being insufficient to capture the model performance where the distribution matches well but yields very low R^2 and vice versa.

Unlike its insignificant impact on the model performance for idealised layouts in Sect. 3.1, the prevailing wind direction greatly affects the model performance in the first row of Fig. 7. This can be traced back to different prevailing wind directions changing the windward and leeward pairing of buildings, which then produce wind extremes at completely different regions. For the $\alpha = 0^o$ configuration, the prediction model produces two false positives at the building edges in the upper panel, which is perhaps affected by the training data with other prevailing wind directions (which has more wind extremes, $\alpha = 30^o$ for example).

The second row considers both the impact of wind direction and building height distribution in a very dense layout. While the prediction model restores the wind field well in the uniform layout, it produced some false positives when adding the actual

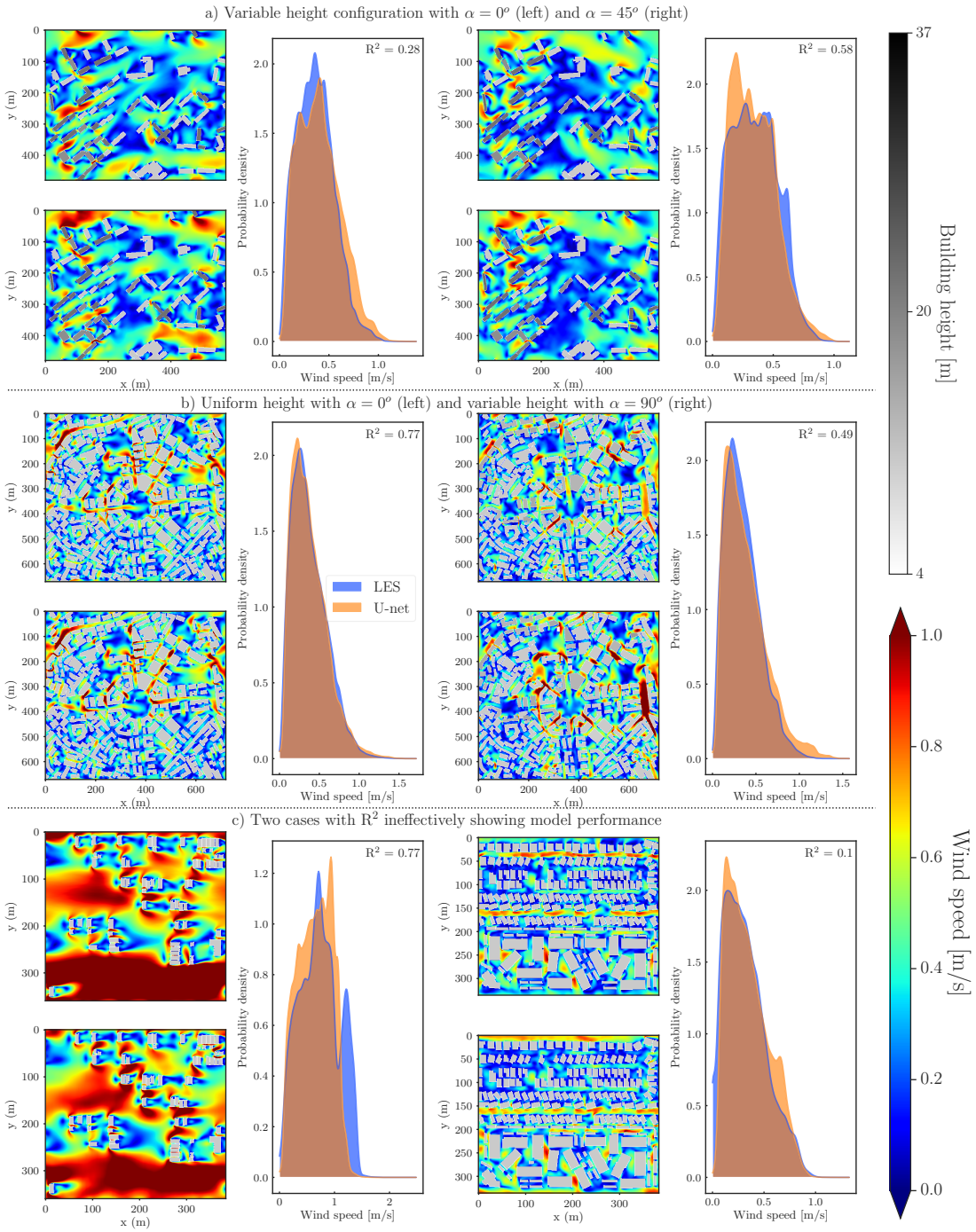

Figure 7: Similar to Fig. 3, but for predictions based on the whole UrbanTALES dataset. The first two pairs are selected to show the impacts of building height configuration and prevailing wind direction on the model performance, and the third pair shows two examples where the R^2 cannot fully reflect model performance. Six cases are presented, with configurations and angles indicated by the vertical titles. Height and wind speed colour bars are shared between the LES results and U-net predictions for each case.

building height distribution. This could be explained by the NN model correlating the long unobstructed streets along with the wind direction to the high wind speed region, which is consistent with (Lu et al., 2023a). However, the correlation is not true in some cases where the upstream layout is blocking the incoming wind.

Finally, we select the two cases in the third row to illustrate the R^2 coefficient being insufficient to reflect model performance. The left panel demonstrates a wind speed field with a double-peak distribution, which is beyond consideration of some wind speed estimation approaches based on simple distribution functions (Wang et al., 2024). The prediction model shows a higher R^2 score but the wind speed distribution is poorly captured where the fast wind speed region is underestimated in both size and value. This can be concerning if one accepts the prediction quality from high R^2 but both extremes and distribution are missed. The right panel shows a case where the distribution is captured better than the R^2 indicates, where the windward fast wind is predicted. The above two examples demonstrate that R^2 does not fully reflect prediction quality and has to be considered with metrics based on wind statistics and distribution as used in the present study.

The ML model built on the entire UrbanTALES provides a full urban representation other than the common yet simple urban canyon (Harman et al., 2004) model. This will benefit both higher resolution climate modelling practice touching the urban scale (Chen et al., 2022b) and trends of analysing urban climate based on realistic urban geometry pattern (Yang et al., 2024).

4. Conclusions

We proposed an efficient ML approach to estimate the pedestrian-level wind field over the complex urban environment featuring a great geometry heterogeneity. The model demonstrates excellent capacity in predicting wind patterns and statistics, having been trained on the comprehensive LES dataset, UrbanTALES (Nazarian et al., 2024), which covers both idealised and realistic urban configurations. Wind extremes, with the lowest typically occurring on the building's leeward facets and the highest in the wake (Oke et al., 2017), are also sufficiently tracked, though the magnitude is underestimated in some configurations.

Urban environment studies rely on different aspects of the wind speed field and therefore the prediction model requires a multi-faceted evaluation. While the agreement in the probability density function reflects both prediction capacity in mean and extreme wind, the determination coefficient R^2 is not sufficient in reflecting either. The proposed approach offers intrinsic advantages over statistical models (Wang et al., 2024) and regression models with comparable computational demands, particularly in handling complex, realistic flow fields. This is achieved by allowing the model to learn the entire flow field without relying on unrealistic assumptions, such as predefined distribution functions.

The proposed model demonstrates the capacity of ML model in predicting complex

urban phenomena by learning the image pattern without resolving the actual physical processes. The model is not constrained to only predict a horizontal slice of the urban wind field. While the full 3D urban field speed is also available in UrbanTALES, the model can be tuned to replace urban canopy models (Lu et al., 2024a) in characterizing urban environment interaction and flow exchange with the atmosphere. Other urban climate variables such as mean radiant temperature can also be predicted in the same way given the dataset is available (Briegel et al., 2023).

There are several promising directions for future work from both the expansion of the host urban airflow dataset and the ML model development. First, it is expected supplementing realistic urban neighbourhoods under different meteorological conditions improves the model performance more than fully idealised configurations (Javanroodi et al., 2022). Meanwhile, the choice of realistic neighbourhoods in the dataset should leverage the targeted city, where the geometrical condition can be further classified and generalised to minimise the scenarios required Boeing, 2019. From the model development perspective, the prediction capacity of wind extreme could be improved by incorporating a quantile loss term into the loss function, which penalises the model for incorrect predictions of the extreme quantiles (Bittner et al., 2023)). Finally, having more realistic urban features to the input such as digital surface model (DSM), vegetation (Vatani et al., 2024), and thermal forcings to emulate the multiphysical flow field, is also an extension.

Acknowledgements

This research was supported by the Australian Research Council Centre of Excellence for Climate Extremes (Grant CE170100023). Simulations were undertaken with the assistance of resources and services from the Australian Government's National Collaborative Research Infrastructure Strategy (NCRIS), with access to computational resources provided by the National Computational Infrastructure (NCI), which is supported by the Australian Government through the National Computational Merit Allocation Scheme.

Data Availability Statement

The related training data, scripts and output are stored in https://doi.org/10.5281/zenodo.12749995. The description of each file in the repository is listed as follows:

- `topo.zip`: The input data for the U-net model, i.e., urban geometries and configurations. This file will be available upon the paper's publication.
- `wind.zip`: The output data for the U-net model, i.e., magnitude of wind speed from LES simulations. This file will be made public upon the paper's publication.
- `data_formatter.py`: The Python script for data processing.

- `idea_var_cases_20exp.zip`: The metrics for U-net predictions from 20 experiments with different data split seeds, using only the idealised-variable data.
- `idea_var_cases_1exp.zip`: The U-net predictions for the test set from a specific experiment, using only the idealised-variable data.
- `all_cases_20exp.zip`: The metrics for U-net predictions from 20 experiments with different data split seeds, using all the data.
- `all_cases_1exp.zip`: The U-net predictions for the test set from a specific experiment, using all the data.

Appendix A. Adjustment to the Generic U-net Model

To speed up the training, reduce memory usage, and ensure physical soundness of the prediction, we have applied the following adjustments to the original generic U-net model:

(i) We added two additional max-pooling operations, which downsample by taking the maximum value in each region, to further reduce the spatial information;

(ii) We increased the number of feature channels by 16 in each convolutional operation, a process that applies filters to extract features, following a max-pooling layer, instead of by 64;

(iii) We added batch normalisation, a technique that standardises layer inputs, after each 3×3 convolutional layer to prevent gradient explosion during training;

(iv) We applied an additional Rectified Linear Unit (ReLU) activation after the final 1×1 convolution layer to ensure that the output, representing the wind speed magnitude, remains non-negative.

Appendix B. Procedures transferring information between LES raw flow field and ML workflow

Starting from the raw LES flow field, we proceed with the expansion and slicing as data pre-processing steps shown in Fig. 1(c). For example, the input urban geometry depicted in Fig. 1(c) has an original size of 432×576, while we set 400×400 as the input size of the U-net model. The procedure to keep image size uniformity is: to expand the image to 800×800, followed by slicing the expanded image into four 400×400 patches. For other prevailing wind directions, i.e., α not divisible by 90, the pre-processing steps consist of expansion, rotating, cropping, and slicing. Under this context, two technical considerations arise:

(i) It is crucial to ensure the expanded image maintains periodicity along boundaries before rotation, as the image undergoes a secondary expansion during the rotation process;

(ii) During post-processing, when reverse-rotating the formatted image to restore the prediction for the original input, it is essential to ensure the integrity of the recovered image.

For example, as shown in Fig. 1(d), given an image size of 240×400 with $\alpha = 45^o$ and a target size of 320×320, we first need to determine the number and arrangement of original images. In this regard, 2×2 arrangements can fulfil consideration in (ii). It's worth noting that using a decimal image number, e.g., 2.5×2 instead of 2×2, is invalid as it breaks the periodicity of the boundary and thus consideration (i) is not fulfilled. Subsequently, the original image can be expanded to 480×800 by taking advantage of the periodic boundary conditions. Note that in this case, the expanded image maintains the periodicity along the boundary even though its boundary may not align with the original image's boundary. Thus, consideration (i) is properly handled. Next, we rotate the expanded image by 45 degrees counterclockwise. During the rotation, the image undergoes a second expansion as it wraps around the opposite boundary. The resulting image is then cropped to a size of 640×640, and finally, the cropped image is sliced into four 320×320 patches.

To perform post-processing on the pre-processing depicted in Fig. 1(c), we first stitch the four 320×320 patches to form a 640×640 image. Then, we rotate the output image by α degrees clockwise, and finally, we locate the position of the original image within the rotated image and crop to extract an image of the original size.

Appendix C. Robustness test over different seeding

Below are two figures showing the robustness test on seeding for test only based on idealised building blocks and the entire UrbanTALES dataset, respectively.

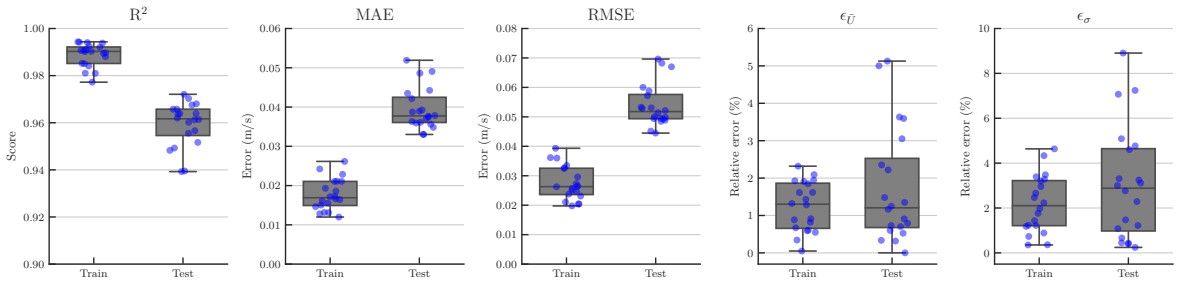

Figure C1: Box plots showcasing the distribution of model performance metrics across 20 experiments within the training and test sets, corresponding to 20 different data split seeds. Each blue circle represents a single experiment trained using the idealised data.

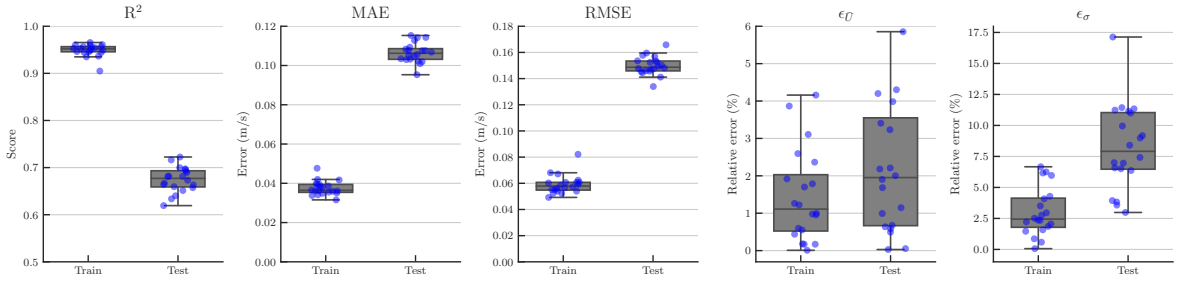

Figure C2: Box plots showcasing the distribution of model performance metrics across 20 experiments within the training and test sets, corresponding to 20 different data split seeds. Each blue circle represents a single experiment trained using the whole dataset.

References

Li, R., Sun, T., Ghaffarian, S., Tsamados, M., and Ni, G. (June 2024). "GLAMOUR: GLobAl building MOrphology dataset for URban hydroclimate modelling". In: *Scientific Data* 11.1, p. 618. DOI: 10.1038/s41597-024-03446-2.

Lu, J., Nazarian, N., Hart, M. A., Krayenhoff, E. S., and Martilli, A. (2024a). "A one-dimensional urban flow model with an eddy-diffusivity mass-flux (EDMF) scheme and refined turbulent transport (MLUCM v3.0)". In: *Geoscientific Model Development* 17.7, pp. 2525–2545. DOI: 10.5194/gmd-17-2525-2024.

Lu, J., Nazarian, N., Hart, M. A., Krayenhoff, E. S., and Martilli, A. (2024b). "Representing the effects of building height variability on urban canopy flow". In: *Quarterly Journal of the Royal Meteorological Society* 150.758, pp. 46–67. DOI: https://doi.org/10.1002/qj.4584.

Nazarian, N., Lu, J., Martilli, A., Lipson, M., Hart, M. A., and Krayenhoff, E. S. (2024). "UrbanTALES: A comprehensive dataset of Urban Turbulent Airflow using systematic Large Eddy Simulations (LES)". In: *Earth System Science Data*.

Vatani, M., Kiani, K., Mahdavinejad, M., and Georgescu, M. (June 2024). "Evaluating the effects of different tree species on enhancing outdoor thermal comfort in a post-industrial landscape". In: *Environmental Research Letters* 19.6, p. 064051. DOI: 10.1088/1748-9326/ad49b7.

Wang, W., Sekikawa, T., Okaze, T., and Ikegaya, N. (July 2024). "Comparison of various statistical methods for estimating extreme wind speed at the pedestrian level in idealized and actual urban areas". In: *Journal of Wind Engineering and Industrial Aerodynamics* 250, p. 105778. DOI: 10.1016/j.jweia.2024.105778.

Yang, L., Yang, Y., Shen, Y., Yang, J., Zheng, G., Smith, J., and Niyogi, D. (May 2024). "Urban development pattern's influence on extreme rainfall occurrences". In: *Nature Communications* 15.1, p. 3997. DOI: 10.1038/s41467-024-48533-5.

Azorin-Molina, C. et al. (July 2023). "Biases in wind speed measurements due to anemometer changes". In: *Atmospheric Research* 289, p. 106771. DOI: 10.1016/j.atmosres.2023.106771.

Bittner, M., Hobeichi, S., Zawish, M., Diatta, S., Ozioko, R., Xu, S., and Jantsch, A. (2023). "An LSTM-based Downscaling Framework for Australian Precipitation Projections". In: *NeurIPS 2023 Workshop on Tackling Climate Change with Machine Learning*.

Briegel, F., Wehrle, J., Schindler, D., and Christen, A. (July 2023). *High-resolution multi-scaling of outdoor human thermal comfort and its intra-urban variability based on machine learning*. preprint. Atmospheric sciences. DOI: 10.5194/gmd-2023-122.

Chockalingam, G., Afshari, A., and Vogel, J. (Feb. 2023). "Characterization of Non-Neutral Urban Canopy Wind Profile Using CFD Simulations—A Data-Driven Approach". In: *Atmosphere* 14.3, p. 429. DOI: 10.3390/atmos14030429.

Herfort, B., Lautenbach, S., Porto De Albuquerque, J., Anderson, J., and Zipf, A. (July 2023). "A spatio-temporal analysis investigating completeness and inequalities of global urban building data in OpenStreetMap". In: *Nature Communications* 14.1, p. 3985. DOI: 10.1038/s41467-023-39698-6.

Lu, J., Nazarian, N., Hart, M. A., Krayenhoff, E. S., and Martilli, A. (2023a). "Novel Geometric Parameters for Assessing Flow Over Realistic Versus Idealized Urban Arrays". In: *Journal of Advances in Modeling Earth Systems* 15.7. e2022MS003287 2022MS003287, e2022MS003287. DOI: https://doi.org/10.1029/2022MS003287.

Lu, Y., Zhou, X.-H., Xiao, H., and Li, Q. (Jan. 2023b). "Using Machine Learning to Predict Urban Canopy Flows for Land Surface Modeling". In: *Geophysical Research Letters* 50.1, e2022GL102313. DOI: 10.1029/2022GL102313.

Chen, S. and Dipankar, A. (2022a). "On the applicability of urban canopy parametrization in building grey zone". In: *Quarterly Journal of the Royal Meteorological Society* 148.745, pp. 1644–1662. DOI: https://doi.org/10.1002/qj.4269.

— (Apr. 2022b). "On the applicability of urban canopy parametrization in building grey zone". In: *Quarterly Journal of the Royal Meteorological Society* 148.745, pp. 1644–1662. DOI: 10.1002/qj.4269.

Javanroodi, K., Nik, V. M., Giometto, M. G., and Scartezzini, J.-L. (July 2022). "Combining computational fluid dynamics and neural networks to characterize microclimate extremes: Learning the complex interactions between meso-climate and urban morphology". In: *Science of The Total Environment* 829, p. 154223. DOI: 10.1016/j.scitotenv.2022.154223.

Liu, K., Lian, Z., Dai, X., and Lai, D. (June 2022). "Comparing the effects of sun and wind on outdoor thermal comfort: A case study based on longitudinal subject tests in cold climate region". In: *Science of The Total Environment* 825, p. 154009. DOI: 10.1016/j.scitotenv.2022.154009.

Lu, J., Nazarian, N., and Hart, M. (May 2022). *OSM2LES - A python-based tool to prepare realistic urban geometry for LES simulation from OpenStreetMap [Software]*. Version 0.1.0. DOI: 10.5281/zenodo.6566346.

Middel, A., Nazarian, N., Demuzere, M., and Bechtel, B. (May 2022). "Urban Climate Informatics: An Emerging Research Field". In: *Frontiers in Environmental Science* 10, p. 867434. DOI: 10.3389/fenvs.2022.867434.

Wang, W. and Okaze, T. (Feb. 2022). "Statistical analysis of low-occurrence strong wind speeds at the pedestrian level around a simplified building based on the Weibull distribution". In: *Building and Environment* 209, p. 108644. DOI: 10.1016/j.buildenv.2021.108644.

Cao, Y. and Huang, X. (Oct. 2021). "A deep learning method for building height estimation using high-resolution multi-view imagery over urban areas: A case study of 42 Chinese cities". In: *Remote Sensing of Environment* 264, p. 112590. DOI: 10.1016/j.rse.2021.112590.

Duan, G. and Takemi, T. (Jan. 2021). "Gustiness in thermally-stratified urban turbulent boundary-layer flows and the influence of surface roughness". In: *Journal of Wind Engineering and Industrial Aerodynamics* 208. Publisher: Elsevier BV, p. 104442. DOI: 10.1016/j.jweia.2020.104442.

Krayenhoff, E. S. et al. (May 2021). "Cooling hot cities: a systematic and critical review of the numerical modelling literature". In: *Environmental Research Letters* 16.5, p. 053007. DOI: 10.1088/1748-9326/abdcf1.

Lin, D., Khan, B., Katurji, M., Bird, L., Faria, R., and Revell, L. E. (May 2021). "WRF4PALM v1.0: a mesoscale dynamical driver for the microscale PALM model system 6.0". In: *Geoscientific Model Development* 14.5, pp. 2503–2524. DOI: 10.5194/gmd-14-2503-2021.

Mokhtar, S., Beveridge, M., Cao, Y., and Drori, I. (Nov. 2021). "Pedestrian Wind Factor Estimation in Complex Urban Environments". In: *Proceedings of the 13th Asian Conference on Machine Learning*.

Sirko, W. et al. (2021). "Continental-Scale Building Detection from High Resolution Satellite Imagery". In: *CoRR* abs/2107.12283.

Wang, W., Wang, X., and Ng, E. (Mar. 2021). "The coupled effect of mechanical and thermal conditions on pedestrian-level ventilation in high-rise urban scenarios". In: *Building and Environment* 191, p. 107586. DOI: 10.1016/j.buildenv.2021.107586.

Ha, J., Choi, Y., Lee, S., and Oh, K. (Jan. 2020). "Diurnal and Seasonal Variations in the Effect of Urban Environmental Factors on Air Temperature: A Consecutive Regression Analysis Approach". In: *International Journal of Environmental Research and Public Health* 17.2, p. 421. DOI: 10.3390/ijerph17020421.

Liu, S. and Shi, Q. (June 2020). "Local climate zone mapping as remote sensing scene classification using deep learning: A case study of metropolitan China". In: *ISPRS Journal of Photogrammetry and Remote Sensing* 164, pp. 229–242. DOI: 10.1016/j.isprsjprs.2020.04.008.

Maronga, B. et al. (2020). "Overview of the PALM model system 6.0". In: *Geoscientific model development* 13.3. 12.02.04; LK 01, pp. 1335–1372. DOI: 10.5194/gmd-13-1335-2020.

Nazarian, N., Krayenhoff, E. S., and Martilli, A. (Mar. 2020). "A one-dimensional model of turbulent flow through "urban" canopies (MLUCM v2.0): updates based on large-eddy simulation". In: *Geoscientific Model Development* 13.3, pp. 937–953. DOI: 10.5194/gmd-13-937-2020.

Takemi, T., Yoshida, T., Horiguchi, M., and Vanderbauwhede, W. (June 2020). "Large-Eddy-simulation analysis of airflows and strong wind hazards in urban areas". In: *Urban Climate* 32, p. 100625. DOI: 10.1016/j.uclim.2020.100625.

Wang, J.-W., Yang, H.-J., and Kim, J.-J. (Oct. 2020). "Wind speed estimation in urban areas based on the relationships between background wind speeds and morphological parameters". In: *Journal of Wind Engineering and Industrial Aerodynamics* 205, p. 104324. DOI: 10.1016/j.jweia.2020.104324.

Boeing, G. (Dec. 2019). "Urban spatial order: street network orientation, configuration, and entropy". In: *Applied Network Science* 4.1, p. 67. DOI: 10.1007/s41109-019-0189-1.

Creutzig, F. et al. (2019). "Upscaling urban data science for global climate solutions". In: *Global Sustainability* 2, e2. DOI: 10.1017/sus.2018.16.

Nazarian, N., Acero, J., and Norford, L. (May 2019). "Outdoor thermal comfort autonomy: Performance metrics for climate-conscious urban design". In: *Building and Environment* 155, pp. 145–160. DOI: 10.1016/j.buildenv.2019.03.028.

Paszke, A. et al. (2019). *PyTorch: An Imperative Style, High-Performance Deep Learning Library*. DOI: 10.48550/arXiv.1912.01703.

Droste, A. M., Steeneveld, G. J., and Holtslag, A. A. M. (Sept. 2018). "Introducing the urban wind island effect". In: *Environmental Research Letters* 13.9, p. 094007. DOI: 10.1088/1748-9326/aad8ef.

Lam, C. K. C., Gallant, A. J., and Tapper, N. J. (Mar. 2018). "Perceptions of thermal comfort in heatwave and non-heatwave conditions in Melbourne, Australia". In: *ICUC9: The 9th International Conference on Urban Climate* 23, pp. 204–218. DOI: 10.1016/j.uclim.2016.08.006.

Lipson, M. J., Thatcher, M., Hart, M. A., and Pitman, A. (July 2018). "A building energy demand and urban land surface model". In: *Quarterly Journal of the Royal Meteorological Society* 144.714, pp. 1572–1590. DOI: 10.1002/qj.3317.

Mei, D., Wen, M., Xu, X., Zhu, Y., and Xing, F. (Oct. 2018). "The influence of wind speed on airflow and fine particle transport within different building layouts of an industrial city". In: *Journal of the Air & Waste Management Association* 68.10, pp. 1038–1050. DOI: 10.1080/10962247.2018.1465487.

Kingma, D. P. and Ba, J. (2017). *Adam: A Method for Stochastic Optimization*. DOI: 10.48550/arXiv.1412.6980.

Oke, T. R., Mills, G., Christen, A., and Voogt, J. A. (Sept. 2017). *Urban Climates*. 1st ed. Cambridge University Press. DOI: 10.1017/9781139016476.

OpenStreetMap contributors (2017). *Planet dump retrieved from https://planet.osm.org*. https://www.openstreetmap.org.

Santiago, J., Borge, R., Martin, F., Paz, D. de la, Martilli, A., Lumbreras, J., and Sanchez, B. (Jan. 2017). "Evaluation of a CFD-based approach to estimate pollutant distribution within a real urban canopy by means of passive samplers". In: *Science of The Total Environment* 576, pp. 46–58. DOI: 10.1016/j.scitotenv.2016.09.234.

Biljecki, F., Ledoux, H., and Stoter, J. (2016). "An improved LOD specification for 3D building models". In: *Computers, Environment and Urban Systems*, pp. 25–37. DOI: 10.1016/j.compenvurbsys.2016.04.005.

Best, M. J. et al. (2015). "The Plumbing of Land Surface Models: Benchmarking Model Performance". In: *Journal of Hydrometeorology* 16.3, pp. 1425–1442. DOI: 10.1175/JHM-D-14-0158.1.

Ronneberger, O., Fischer, P., and Brox, T. (2015). "U-Net: Convolutional Networks for Biomedical Image Segmentation". In: *Medical Image Computing and Computer-Assisted Intervention – MICCAI 2015*. Ed. by N. Navab, J. Hornegger, W. M. Wells, and A. F. Frangi. Cham: Springer International Publishing, pp. 234–241. DOI: 10.1007/978-3-319-24574-4_28.

Kanda, M., Inagaki, A., Miyamoto, T., Gryschka, M., and Raasch, S. (Aug. 2013). "A New Aerodynamic Parametrization for Real Urban Surfaces". In: *Boundary-Layer Meteorology* 148.2, pp. 357–377. DOI: 10.1007/s10546-013-9818-x.

Santiago, J. L., Coceal, O., and Martilli, A. (Oct. 2013). "How to Parametrize Urban-Canopy Drag to Reproduce Wind-Direction Effects Within the Canopy". In: *Boundary-Layer Meteorology* 149.1, pp. 43–63. DOI: 10.1007/s10546-013-9833-y.

Bechtel, B., Zakšek, K., and Hoshyaripour, G. (Oct. 2012). "Downscaling Land Surface Temperature in an Urban Area: A Case Study for Hamburg, Germany". In: *Remote Sensing* 4.10, pp. 3184–3200. DOI: 10.3390/rs4103184.

Letzel, M. O., Helmke, C., Ng, E., An, X., Lai, A., and Raasch, S. (Dec. 2012). "LES case study on pedestrian level ventilation in two neighbourhoods in Hong Kong". In: *Meteorologische Zeitschrift* 21.6, pp. 575–589. DOI: 10.1127/0941-2948/2012/0356.

Yuan, C. and Ng, E. (Apr. 2012). "Building porosity for better urban ventilation in high-density cities – A computational parametric study". In: *Building and Environment* 50, pp. 176–189. DOI: 10.1016/j.buildenv.2011.10.023.

Ng, E., Yuan, C., Chen, L., Ren, C., and Fung, J. C. (May 2011). "Improving the wind environment in high-density cities by understanding urban morphology and surface roughness: A study in Hong Kong". In: *Landscape and Urban Planning* 101.1, pp. 59–74. DOI: 10.1016/j.landurbplan.2011.01.004.

Xie, Z.-T., Coceal, O., and Castro, I. P. (Oct. 2008). "Large-Eddy Simulation of Flows over Random Urban-like Obstacles". In: *Boundary-Layer Meteorology* 129.1, pp. 1–23. DOI: 10.1007/s10546-008-9290-1.

Coceal, O., Thomas, T. G., and Belcher, S. E. (Oct. 2007). "Spatial Variability of Flow Statistics within Regular Building Arrays". In: *Boundary-Layer Meteorology* 125.3, pp. 537–552. DOI: 10.1007/s10546-007-9206-5.

Harman, I. N., Barlow, J. F., and Belcher, S. E. (2004). "SCALAR FLUXES FROM URBAN STREET CANYONS. PART II: MODEL". In.

Martilli, A., Clappier, A., and Rotach, M. W. (Aug. 2002). "An Urban Surface Exchange Parameterisation for Mesoscale Models". In: *Boundary-Layer Meteorology* 104.2, pp. 261–304. DOI: 10.1023/A:1016099921195.